Regionalization of Monthly Rainfall Erosivity Patterns in Switzerland

Simon Schmidt[1], Christine Alewell[1], Panos Panagos[2], Katrin Meusburger[1]

[1]Environmental Geosciences, University Basel, Bernoullistrasse 30, CH-4056 Basel, Switzerland
[2]European Commission, Joint Research Centre, Institute for Environment and Sustainability, Via E. Fermi 2749, I-21027 Ispra, Italy

Correspondence to: Simon Schmidt (si.schmidt@unibas.ch)

Abstract. One major controlling factor of water erosion is rainfall erosivity, which is quantified as the product of total storm energy and maximum 30-min intensity (I_{30}). Rainfall erosivity is often expressed as R-factor in soil erosion risk models like the Universal Soil Loss Equation (USLE) and its revised version (RUSLE). As rainfall erosivity is closely correlated with rainfall amount and intensity, the rainfall erosivity of Switzerland can be expected to have a characteristic regional and seasonal dynamic throughout the year. This intra-annual variability was mapped by a monthly modelling approach to assess simultaneously spatial and monthly patterns of rainfall erosivity. So far only national seasonal means and regional annual means exist for Switzerland. We used a network of 87 precipitation gauging stations with a 10-minute temporal resolution to calculate long-term monthly mean R-factors. Stepwise generalized linear regression (GLM) and leave-one-out cross-validation (LOOCV) were used to select spatial covariates which explain the spatial and temporal patterns of the R-factor for each month across Switzerland. The monthly R-factor is mapped by summarizing the predicted R-factor of the regression equation and the corresponding residues of the regression which are interpolated by ordinary kriging (Regression-Kriging). As spatial covariates, a variety of precipitation indicator data has been included like snow depths, a combination product of hourly precipitation measurements and radar observations (CombiPrecip), daily alpine precipitation (EURO4M-APGD) and monthly precipitation sums (RhiresM). Topographic parameters (elevation, slope) were also significant explanatory variables for single months. The comparison of the 12 monthly rainfall erosivity maps showed a distinct seasonality with highest rainfall erosivity in summer (June, July, and August) influenced by intense rainfall events. Winter months have lowest rainfall erosivity. A proportion of 62% of the total annual rainfall erosivity is identified within four months only (June to September). Highest erosion risk can be expected for July where not only rainfall erosivity but also erosivity density is high. In addition to the intra-annual temporal regime, a spatial variability of this seasonality was detectable between different regions of Switzerland. The assessment of the dynamic behavior of the R-factor is valuable for the identification of susceptible seasons and regions.

Keywords: cumulative daily R-factor, erosion modelling, dynamic soil erosion risk assessment, monthly erosivity

1 Introduction

Soil erosion by water is a major environmental issue in Switzerland which has been measured (Konz et al., 2012, Alewell et al., 2014), mapped (Mosimann, 1990; Prasuhn, 2011; Prasuhn, 2012), and modelled (Gisler et al., 2011; Prasuhn et al., 2013) extensively. In Switzerland, since the 1950s, soil erosion by water is increasing under arable land (Weisshaidinger & Leser, 2006) as well as in mountain grasslands (Meusburger & Alewell, 2008). Mosimann et al. (1991) assessed a quantity of up to 20% of all cultivated land in Switzerland to be affected by soil erosion. The costs of soil erosion for Switzerland's arable land were estimated to be about 53 million CHF yr^{-1} (US $55.2 million yr^{-1}; Ledermann, 2012). Increasing trends of water erosion are predicted for Switzerland under future climate change due to more frequent and heavy precipitation during winter month (Fuhrer et al., 2006). Trends towards increasing rainfall erosivity are already observable in the months May to October (Meusburger et al., 2012).

Rainfall has direct impacts on soil mobilization by processes like rapid wetting or splash and runoff effects and is, therefore, one of the main driving forces of water erosion. The R-factor, as one of the five soil erosion risk factors (rainfall erosivity, soil erodibility, slope steepness and length, cover management, and support practices) of the Revised Universal Soil Loss Equation (RUSLE) (Renard et al., 1997; Foster et al., 2008) expresses the impact of rainfall on soils in form of rainfall erosivity. The RUSLE is widely used for calculating soil loss, but each of the 5 factors also has an essential message on its own. For instance, besides being an important driving factor of soil erosion, the R-factor can also be used to conclude on soil vulnerability, flood hazard, natural hazards, or probability of droughts (Panagos et al., 2015).

Previously published studies on rainfall erosivity in Switzerland focused on national seasonal means (Panagos et al., 2015) or regional annual means (Friedli, 2006; Gisler et al., 2011; Meusburger et al. 2012; Prasuhn et al., 2013;). Since Switzerland has a high spatial climate variability (humid continental to oceanic climate; Köppen, 1936), seasonal and temporal variations of the weather are consequential. As such, these spatio-temporal climate variations can be expected to influence patterns in the rainfall erosivity. Spatial and temporal patterns of R-factors have not yet been established and mapped for Switzerland although Meusburger et al. (2012) already showed the presence of a strong seasonality of the rainfall erosivity for stations clustered at different elevation classes in Switzerland. So far the lack of significant spatial covariates impeded the mapping of intra-annual rainfall erosivity patterns. The availability of hourly radar rainfall observations for Switzerland (CombiPrecip data; Sideris et al., 2014) might offer a new possibility for the modelling of rainfall erosivity maps for individual months. These spatio-temporal patterns are decisive in combination with spatio-temporal patterns of vegetation cover in order to allow for an accurate soil erosion risk assessment and relevant for a monthly and seasonal management of agriculture practices and hazard controls. A rather static approach which aggregates either regionally or temporally R-factors like it was presented by Meusburger et al. (2012) is not suitable to model the dynamic soil erosion risk on a seasonal scale. Furthermore, the impact of precipitation on rainfall erosivity can be assessed by determining the monthly erosivity density. Here, we aim to assess the spatio-temporal variability of rainfall erosivity in Switzerland by

(i)   extending the network of gauging stations from Meusburger et al. (2012) to obtain rainfall erosivity events for Switzerland

(ii)   producing monthly R-factor maps based on high resolution spatial covariates using a regression-kriging approach

(iii)   evaluating the spatio-temporal patterns of the seasonal R-factor dynamics and

(iv)   determining the spatio-temporal erosivity density in Switzerland.

2 Material and Methods

2.1 Rainfall erosivity (R-factor) calculation

The rainfall erosivity expressed as R-factor in RUSLE is the summation of the total storm energy (E) of an erosive rainfall event times its corresponding maximum intensity over a time span of 30-minutes (I_{30}) within a certain time period (Brown & Foster, 1987). We used the erosive rainfall event thresholds defined by Renard et al. (1997) which were modified by Meusburger et al. (2012). The unit rainfall energy (e_r) (MJ ha^{-1} mm^{-1}) for each time interval is expressed as the intensity of rainfall (i_r) (mm h^{-1}) during that time interval. It is calculated by Brown and Foster (1987) as:

$$e_r = 0.29[1 - 0.72 \exp(-0.05 i_r)] \tag{1}$$

The erosive rainfall event erosivity (EI_{30}) (MJ mm ha^{-1} h^{-1}) is a product of the unit rainfall energy (e_r) (Eq. (1)) and its maximum rainfall amount within a 30-minutes interval (according to Wischmeier & Smith, 1978):

$$EI_{30} = (\sum_{r=1}^{k} e_r v_r) I_{30} \tag{2}$$

where v_r is the rainfall volume (mm) during a time unit r and I_{30} is the maximum rainfall intensity within 30-minutes of the event (mm h^{-1}).

The monthly rainfall erosivity (R_{mo}) (MJ mm ha^{-1} h^{-1} month^{-1}) is the mean of the accumulated event erosivity (EI_{30}) (Eq. (2)) within a month:

$$R_{mo} = \frac{1}{n} \sum_{j=1}^{n} \sum_{k=1}^{m_j} (EI_{30})_k \tag{3}$$

where n is the recorded number of years with the number of erosive events (m_j) within a certain month j. k is the index of a single event with its corresponding event erosivity.

The event rainfall erosivity was calculated for each station by applying the algorithm of Meusburger et al. (2012) (http://eusoils.jrc.ec.europa.eu/themes/r-factor-switzerland-version-2012). The event rainfall erosivity was averaged by months to a long-term monthly mean R-factor (R_{mo}). Originally, the 30-minute maximum rainfall rate (I_{30}) is obtained by breakpoint precipitation data which is recorded in intervals of fixed rainfall rates instead of fixed time intervals (Wischmeier & Smith, 1978; Hollinger et al., 2002). As stations recording breakpoints are rare in Switzerland, we used records with a fixed time interval of 10-minutes. Using small time intervals better represents breakpoint data and records the intensity more realistic. Longer intervals might underestimate rainfall intensity (Porto, 2016; Panagos et al., 2016a). For time intervals shorter than 15 minutes Porto (2016) reported an overestimation compared to the commonly used $(EI_{30})_{15}$ (15-minutes

interval) and proposed a mean conversion factor of 0.97 for all investigated stations in southern Italy. This rather small deviation can mainly be explained by the fact, that the maximum intensity of the 10-minute record is upscaled to the whole 30-minutes increment. To avoid this bias our algorithm uses a 30-minute moving average to identify the maximum I_{30} and as such resembles the original approach of Wischmeier & Smith (1978) to obtain the I_{30} from "successive increments of essentially uniform intensity" (Wischmeier & Smith, 1978). As we are working with the same 10-minute measuring interval at all 87 stations, no conversion factor was applied to homogenize the data (cf. Agnese et al., 2006; Porto, 2016; Panagos et al., 2016a). Usually, snow, snowmelt and rainfall on frozen soil are not assessed in the R-factor (Renard et al.; 1997). Thus, a temperature threshold of 0°C was set to obtain only rainfall and exclude snow water equivalents which are subject to uncertainty in rainfall erosivity assessments (Leek & Olsen, 2000). Temperature data was measured simultaneous to precipitation (for 71 stations) or was directly derived (for 16 stations) from the closest stations (within a distance of less than 20 km) at similar elevation with an hourly resolution. We assumed only minor variation in temperature within that distance at a similar elevation level.

Besides neglecting snow, we did not consider rainfall as hail which is mainly occurring during summer in Switzerland (Nisi et al., 2016; Punge & Kunz, 2016). Although, Hurni (1978) investigated the impact of hail on rainfall erosivity for single plots in Switzerland and concluded that a water equivalent amount of hail exceeds the one of rainfall, hail erosivity is not yet considered for this study.

2.2 Stations

We extended the gauging station network of Meusburger et al. (2012) (10-minutes measuring intervals) by 23% from 71 to an updated dataset of 87 stations (Fig. 1) and upgraded stations by longer time series if available.

The additional 16 stations were previously investigated for rainfall erosivity by Nogler (2012). On average, the network represents one station each 22 km. The average distance of one station to all others is 113.6 km by a minimum distance to the closest station of 13.2 km and a maximum distance of two stations by 324.6 km. A majority of 72% of all stations (63) have recorded data of at least 22 yr. The mean length of observations is 19.5 yr and thus, meet the proposed minimum time-scale requirements for rainfall erosivity calculations of a 15 yr measuring period (Foster et al. 2008). The stations are well distributed and were subject to a quality control (Begert et al., 2005; Nogler, 2012).

2.3 Data and Covariates

The high intra-annual variability of rainfall erosivity was already discussed in Meusburger et al. (2012), but not be spatio-temporally mapped. The monthly erosivity mapping in a country with a high proportion of remote Alpine areas requests a variety of erosivity influencing covariates. High temporal information on snow cover and snow water equivalents, high spatio-temporal information on rainfall and high spatial information on topography are acquired as covariates (Table 1) for the monthly erosivity maps since rainfall erosivity is mainly controlled by precipitation and relief parameters (Meusburger et al., 2012; Panagos et al., 2015; Panagos et al., 2016b). All spatial covariates have a much higher resolution (spatial and

temporal) than datasets used in previously R-factor studies for Europe (Panagos et al., 2015; 2016a) and Switzerland (Meusburger et al., 2012) and therefore the R-factor mapping is feasible at a higher spatial and temporal precision.

The long-term snow depth (derived from mean monthly snow depth by MeteoSwiss) on a monthly resolution was used as an approximation for precipitation as snow. The monthly point data of snow depth was regionalized by Inverse Distance Weighting. Hourly Swiss CombiPrecip data (geostatistical combination of rain gauge measurements (150 automatic stations) and three C-band radar observations; Sideris et al., 2014) were aggregated and averaged to a long-term monthly mean. Long-term mean daily precipitation per month was calculated based on the daily values of alpine precipitation in EURO4M-APGD (Isotta et al., 2014). Averaging the monthly spatial precipitation of RhiresM (MeteoSwiss, 2013) over the years leads to long-term monthly mean precipitation sums. The variables elevation, slope, and aspect are retrieved from a 2 m Digital Terrain Modell (SwissAlti3D) for Switzerland.

2.4 Mapping the seasonal variability of rainfall erosivity in Switzerland

Hanel et al. (2016) and Angulo-Martínez & Beguería (2009) tested different interpolation methods were tested for Czech Republic (Hanel et al., 2016) and the Ebro Basin in Spain (Angulo-Martínez & Beguería, 2009). Both studies could confirm that a combination of regression and residual kriging (regression-kriging) is among the most suitable methods to interpolate rainfall erosivity. We also used regression-kriging (Hengl et al., 2004; Hengl, 2007; Hengl et al., 2007) to map the monthly variability of rainfall erosivity in Switzerland. The regression-kriging approach employed on the monthly mean rainfall erosivity for each of the 87 stations (R_{mo}). In a first step a generalized linear regression (GLM) (Gotway & Stroup, 1997)is used to establish a regression between R_{mo} and the high resolution covariates. The GLM relates the rainfall erosivity (target variables) to the covariates (Table 1) and predicts rainfall erosivity at the same scale as covariates are available (Odeh et al., 1995; McBratney et al., 2000). In an second step the residuals of the GLM are interpolated by an ordinary global kriging (McBratney et al. 2000; Hengl et al., 2004). Finally, the predicted rainfall erosivity by the GLM is summarized with the residuals map (established by the kriging procedure). The combination of interpolated R_{mo} with the spatial variation of its residuals enables the quantification of the standard error related to the erosivity mapping.

Besides the standard error maps, leave-one-out cross-validation (LOOCV) was used as a second quality check of the mapping procedure (Efron & Tibishirani, 1997). However, data-splitting reduces the training observations and doesn't show the same results by repetition due to bias and randomness (Steyerberg, 2009; Harrell, 2015). In contrast, LOOCV avoids a resampling-bias since it omits only one observation from the dataset per run and estimates the model from the remaining n-1 observations. It yields the same regression coefficients by repetition due its reproducibility (James & Witten, 2015). In contrast, data-split reduces the training observations and doesn't show the same coefficients due to randomness (Steyerberg, 2009; Harrell, 2015). To compensate for the low validation subset, the process was repeated 100 times.

A log-transformation of R_{mo} resulted in a normal distribution of the data. The suitability of each covariate for the GLM was determined by an automated stepwise feature selection process according to the Akaike information criterion (AIC). The α-to-enter significance level for covariate selection was set to 0.1 (Kutner et al., 2005; Gupta & Guttman, 2013). We also

tested Least Absolute Shrinkage and Selection Operator (LASSO) as an alternative feature selection method to the stepwise GLM, but it was less transparent for evaluation and showed inappropriate residual diagnostics (systematic error). Both, the LOOCV stepwise regression, as well as LASSO, were performed in the R-package "caret" (v6.0-68). Outliers (Bonferroni-adjusted outlier test) and influential observations (Cook's Distance) were omitted in the stepwise GLM.

5   The goodness-of-fit of the model was described by the coefficient of determination (R^2), the root mean square error (E_{RMS}) and the deviance. Regression diagnostics to evaluate the model included normality, non-constant error variance (homoscedasticity), multicollinearity (variance inflation factor; vif) and autocorrelation.

Twelve monthly maps of the long-term mean R_{mo} were derived by applying the regression equation with the covariates and their corresponding coefficients according to the individual monthly regression equation. The residuals of each months'

10   stepwise GLM were interpolated by an ordinary global kriging with a stable variogram model and added to the R_{mo} maps in ESRI ArcGIS (v10.2.2.) afterwards.

Each monthly map is subject to an individual GLM. Therefore, a subset of individual covariates explains rainfall erosivity for each month separately. An averaging of three monthly maps leads to long-term seasonal mean R-factor (R_{seas}) maps for Switzerland with high spatial resolution. In addition, the sum of all 12 maps results in an updated (compared to Meusburger

15   et al., 2012) long-term annual mean R-factor (R_{year}) map.

2.5 Cumulative daily R-factors

The averaged cumulative percentage of R-factor within a year is obtained and grouped by Swiss biogeographic regions. The biogeographic regions were selected because they show distinct differences in climate, soils, elevation, steepness, and geographic location. The cumulative curve of rainfall erosivity enables the extraction of the annual share of rainfall erosivity

20   on a daily scale and is required for the calculation of RUSLE C-factors. C-factors are based on the product of the soil loss ratio (for a specific time of the year and a specific crop) and the cumulative percentage of rainfall erosivity of distinct days of the year (Wischmeier & Smith, 1978; Schwertmann et al., 1987; Renard et al., 1997). Therefore, all recorded rainfall events of a certain station within an individual biogeographic unit and at a specified day in the year are averaged over the measuring period and with the other stations of the region on a long-term mean daily level. That calculation of C-factors requires the

25   percentage of the total annual rainfall erosivity of distinct days of the year which can be derived by that procedure.

2.6 Monthly erosivity density

Monthly erosivity density (ED_{mo}) (MJ ha^{-1} h^{-1}) is calculated by the ratio of the long-term R_{mo} (MJ mm ha^{-1} h^{-1} month^{-1}) (neglecting rain as snow) to mean monthly precipitation amount (P_{mo}) (mm month^{-1}) (including rain as snow) according to the equation proposed by Foster et al. (2008):

30   $$ED_{mo} = \frac{R_{mo}}{P_{mo}} \tag{4}$$

Small values (<1) of ED_{mo} indicate that the influence of monthly precipitation on the monthly rainfall erosivity is mainly driven by its amount. On the other hand, high values of ED_{mo} show, that relative to the absolute rainfall amount a high kinetic energy of rainfall was observed (e.g., strong storm events; Panagos et al., 2016b). Highest soil erosion risk is expected for areas where rainfall erosivity is high but related to a few intense rainfall events (high values of ED_{mo}). As such, ED_{mo} can reflect the temporal variability of rainfall intensity (Dabney et al., 2011) and can indicate how precipitation (short duration events with high intensities or high amounts of rainfall) controls the seasonality of rainfall. ED_{mo} was calculated using i) the erosivity (R_{mo87}) and monthly precipitation sums (P_{mo87}) of each station (ED_{mo87}) and ii) the 12 interpolated monthly rainfall erosivity maps R_{mo} and RhiresM as the monthly precipitation dataset (ED_{mo}). RhiresM is an already available precipitation dataset of MeteoSwiss that includes most of the 87 gauging stations. For the spatial mapping of monthly erosivity density, the interpolated monthly datasets R_{mo} and RhiresM were chosen since an interpolation of ED_{mo87} would require additional interpolation methods and spatial covariates which are explanatory for the monthly erosivity density. Additionally, a performed interpolation might still modify the ED_{mo87} in accordance to the values at neighbouring stations. According to Dabney et al. (2012), erosivity density is relatively independent of elevation up to a height of 3000 m a.s.l.. In Switzerland, only the station Piz Corvatsch (COV) exceeds that threshold of height.

3 Results and Discussion

3.1 Monthly rainfall erosivity at the 87 Swiss gauging stations

R_{mo}-data averaged for all investigated stations show a bell-shaped curve over the 12 months (Fig. 2) with an increasing trend starting from February (17.3 MJ mm ha^{-1} h^{-1} month^{-1}) to a maximum in July (289 MJ mm ha^{-1} h^{-1} month^{-1}). The mean R_{mo} per month is 112 MJ mm ha^{-1} h^{-1} month^{-1}. The meteorological season winter (Dec-Jan-Feb) has the lowest mean R_{mo} (33 MJ mm ha^{-1} h^{-1} month^{-1}), followed by spring (Mar-Apr-May) (68 MJ mm ha^{-1} h^{-1} month^{-1}), fall (Sep-Oct-Nov) (92 MJ mm ha^{-1} h^{-1} month^{-1}) and summer (Jun-Jul-Aug) (257 MJ mm ha^{-1} h^{-1} month^{-1}). Most of the monthly R-factors (96%) of the lowest 10% of all monthly values are part of the period between November and April whereas 97% of the highest 10% are monthly rainfall erosivity in the period of May to October.

The "Monthly Rainfall Erosivity" for Europe by Panagos et al. (2016a) and the national observations of Mosimann et al. (1990) for a single station in Switzerland (Bern, Swiss Midland) comply with the present calculations with highest rainfall erosivity for the season from June/July to August. The Swiss monthly rainfall erosivity in the European assessment (Panagos et al., 2016a) are on average by 3 MJ mm ha^{-1} h^{-1} month^{-1} smaller (after rescaling with the calibration factors from 30 to 10 minutes). That discrepancy by 5% mainly arises due to the different numbers and time series of gauging stations (87 vs. 71).

Seasonality of R_{mo} on a continental scale is observed for Europe (Panagos et al., 2016a) and Africa (Vrieling et al., 2014), on a national scale for Brazil (da Silva, 2004), Cape Verde (Mannaerts & Gabriels, 2000), Chile (Bonilla & Vidal, 2011), Denmark (Leek & Olsen, 2000), El Salvador (da Silva et al., 2011), Greece (Panagos et al., 2016b), Iran (Sadeghi et al., 2011; Sadeghi & Hazbavi, 2015; Sadeghi & Tavangar, 2015), Italy (Diodato, 2005; Borrelli et al., 2016), Korea (Lee &

Won, 2013), New Zealand (Klik et al., 2015), and inter alia for regions of Australia (Yang et al., 2015; Yang & Yu, 2015), Belgium (Verstraeten et al., 2006), Brazil (da Silva et al., 2013), Cape Verde (Sanchez-Moreno et al., 2014), China (Jing et al., 2009; Zhu et al., 2011; Wang et al., 2013; Zhao et al., 2015; Lai et al., 2016), England and Wales (Davison et al., 2005), Ethiopia (Meshesha et al., 2015), Japan (Laceby et al., 2015), the Himalayas (Ma et al., 2014), Italia (Terranova & Gariano, 2015), South Korea (Arnhold et al., 2014), Malaysia (Shamshad et al., 2008), Poland (Banasik & Górski, 1993; Banasik et al., 2001), Slovenia (Petkovšek & Mikoš , 2004; Mikoš et al., 2006), Spain (Renschler et al., 1999; Angulo-Martínez & Beguería, 2009), Turkey (Özşahin, 2014) and the United States of America (Wilkes & Sawada, 2005). However, the timing of the maximum and minimum erosivity varies considerably. Some of the above mentioned studies show highest values in fall and winter (e.g. Greece), highest values in March and lowest values in July (e.g. Iran), or highest values in January and lowest values in July (e.g. Australia). The seasonal R_{mo} in Italy and Greece have lower ranges (209 and 121 MJ mm ha^{-1} h^{-1} month^{-1} compared to 272 MJ mm ha^{-1} h^{-1} month^{-1} in Switzerland), and the peak of the R-factor is shifted from July to September for Italy and to November for Greece, respectively.

3.2 Mapping of monthly rainfall erosivity and related uncertainties

All covariates – aspect excluded – were significant (p-value < 0.1) within the stepwise regressions for at least one month to explain R_{mo} (Table 2). For each month, an individual selection of covariates was achieved by the stepwise GLM. The higher the ratio of the null deviance to the residual deviance, the better the model fits by including the covariates. The residual deviance is lower than the null deviance in all 12 investigated months. Monthly model efficiency and omitted influential outliers to increase the model's goodness of fit are summarized in Table 3. The monthly observations of R_{mo} at the 87 locations (exclusive outliers) as well as the residuals are normally distributed after the log-transformation. A non-constant error (homoscedasticity), multicollinearity and non-autocorrelation were determined for all observations of the 12 months. H_0, which tests that all error variances are equally, was accepted by the Breusch-Pagan-test in all cases and confirms homoscedasticity. Regression diagnostics further show a vif<4 for each month. Therefore, we could not identify collinear data. According to a Durbin-Watson-test, the Swiss R_{mo}-dataset is not autocorrelated.

Model efficiency, averaged over all 12 months has a mean R^2 of 0.51 and a mean E_{RMS} of 93.27 MJ mm ha^{-1} h^{-1} month^{-1}. Among that period, R^2 varies between 0.10 (Nov) and 0.66 (July). E_{RMS} ranges from 6.98 to 330.16 MJ mm ha^{-1} h^{-1} month^{-1} within a year. Regression functions for November and December are most uncertain with lowest R^2 and highest E_{RMS}. The low R^2 are arising due to the generally low rainfall erosivity in winter that is mainly caused by lower rainfall amounts and higher amounts of snow (neglected in this study), which make it more challenging to predict R. The same constrain was observed in a study for Greece where the lowest R^2 was observed for the month with lowest rainfall erosivity (Panagos et., 2016b). Even though, the spatial erosivity prediction for the winter month related to high uncertainties, the latter will will have little effects on soil erosion assessment since rainfall erosivity has the lowest impact on soils in winter.

After adding the kriging interpolation of the residuals to the regionalization of monthly R-factors (based on the stepwise GLM), R^2 are increased in all months. As such, the regression-kriging improves the prediction of R-factors especially for

months with low R^2 as in the case for November and December. The ranges of the stable variograms exceed the minimum distance (approx. 13.2 km) of neighboring stations in all months. The average prediction error of all 12 months is -0.0055. The used stable semivariogram models are represented by 12 lag classes. Common patterns of increasing standard deviations with distances from gauging stations are recognizable in the standard deviation maps.

3.3 Monthly rainfall erosivity maps for Switzerland

Regionalized temporal patterns of modelled R_{mo} show a distinct seasonality with national means being lowest in January (10.5 MJ mm ha^{-1} h^{-1} month^{-1}) and highest in August (263.5 MJ mm ha^{-1} h^{-1} month^{-1}) (Table 4 and Fig. 3). Fig. 3 represents R_{mo} on a stretch between 0 and 200 MJ mm ha^{-1} h^{-1} month^{-1} for a better spatial comparison of the colour schemes although the R-factors are higher than 200 MJ mm ha^{-1} h^{-1} month^{-1} in summer (cf. Table 4). Winter is the season (Fig. 4) with the lowest rainfall erosivity. The highest R_{mo} peak in summer is consistent with the map of extreme point rainfall of 1h duration (100-year return period; Spreafico & Weingartner, 2005), where the strong influence of extreme rainfall events on rainfall erosivity is indicated. Meusburger et al. (2012) already pointed to the relationship of thunderstorm activity to annual rainfall erosivity. The thunderstorm season in Switzerland lasts from late spring (May) to early fall (September). Thunderstorms are at least partly responsible for the high values of rainfall erosivity in summer. Starting from early fall (September), a decreasing trend of R_{mo} is noticeable all over Switzerland.

Averaged months are aggregated to representative seasons (R_{seas}) to identify spatial differences (Fig. 4). Spatially, mean winter rainfall erosivity show highest values in the Jura Mountains, western and eastern parts of the Northern Alps and the Southern Alps (canton Ticino). High winter rainfall erosivity can be explained by rainfall resulting from low-pressure areas in Northern Europe and weather fronts moved by north-westerly winds. These fronts are uplifted at the Jura Mountains what results in orographic rainfall. In spring, the Northern and the Southern Alps become more affected by high rainfall erosivity. The spatial variability of rainfall erosivity in spring in the Southern Alps (canton Ticino) corresponds to the air flow from the south and the onset of the thunderstorm season in that region which causes intense rainfall. High rainfall erosivity are persisting from spring to fall in the Southern Alps. The generally high summer R-factors in the Southern Alps, the Jura Mountains and the Northern alpine foothill are driven by thunderstorms (van Delden, 2001; Perroud & Barder, 2013; Nisi et al., 2016; Punge & Kunz, 2016) and particularly in the Southern Alps by high intense rainfall originating from orographic uplifts (Schwarb et al. 2001; Perroud & Barder, 2013). The cantons of Valais and Grisons remain with relatively low rainfall erosivity among all seasons due to lower convection and thereby lower rainfall erosivity in summer.

The degree of maximal variation at a certain location along a year (expressed as the difference between minimum and maximum monthly rainfall erosivity of all 12 months; Fig. 5) indicates the highest intra-annual range (up to 6086 MJ mm ha^{-1} h^{-1} month^{-1}) in the canton Ticino at the Southern Alps. Also the Northern Alps, Swiss Midland and Jura Mountains show a high erosivity variation within a year. The Eastern and Western Central Alps have lowest ranges in accordance with their relatively low rainfall erosivity among the year. While the range map displays the absolute values of variation, the coefficient of variation map (ratio of standard deviation to the mean of all 12 months; Fig. S1) indicates the relative degree

of erosivity variation (in percent) at a certain location along a year. According to this map, highest variation of up to 207% can be observed in the Eastern Alps (canton Grisons) were monthly rainfall erosivity is low and standard deviation is high. In the Muamba catchment in Brazil, high seasonal variations are also observed in regions with relatively low rainfall erosivity (da Silva et al., 2013).

5   Compared to the rainfall erosivity evaluation by Meusburger et al. (2012) on an annual scale, the observed mean R_{year} and spatial patterns did only change slightly due to the extended station network and higher resolution spatial covariates (aggregated by all 12 monthly R-factor-maps). Improvements of the new map are the extended network of gauging stations, the cross-validation of the regression-kriging approach, and the inclusion of new high spatio-temporal covariates in order to increase the spatial resolution of the maps.

3.4 Cumulative daily rainfall erosivity

Generally, steepest slopes of the cumulative rainfall erosivity curve for Switzerland can be noticed from June to September with a share of 62% of the total annual rainfall erosivity within these four months (Fig. 6). That proportion complies with the cumulative sum of southwest Slovenia (63,2%; Petkovšek & Mikoš , 2004) and exceeds the average share of Europe of 53% (Panagos et al., 2016a) during the same period. A much larger proportion (90%) of cumulative percentage of daily rainfall

15   erosivity was observed for Bavaria (Schwertmann et al., 1987) and eastern Poland (78%; Banasik & Górski, 1993). Mosimann et al. (1990) showed in a single-station approach (Bern, Swiss Midland) that a proportion of 80% of the total annual erosivity occurs in the period from April to September, which complies with the national share (resulting from the multi-station (87) calculation) of 77% during the same period of a year.

All biogeographic units in Switzerland have similar trends of the cumulative daily rainfall erosivity. However, a Wilcoxon

20   signed rank showed that all pairs of the sum curves of biogeographic regions have significant differences (significance level 0.05). Highest proportions (from Jun to Sep) and, therefore, steepest slopes can be identified for the Southern Alps with a share of 70% of the total sum. This high percentage of rainfall erosivity within a short period of time (four months) is likely to have a large impact on the soil erosion susceptibility since it may coincide with lowest (after harvesting of crops, carrots, etc.) and unstable vegetation cover (after late sowing) (Hartwig & Ammon, 2002; Wellinger et al., 2006; Torriani et al.,

25   2007; Prasuhn, 2011). Furthermore, fully grown pre-harvest field crops (e.g. cereals, maize) might suffer by bend-over of corn stalks due to high intensity storms. In addition, water saturated conditions which are usual in May and September/October makes soils even more erodible. Highly susceptible soils in summer may also be expected in areas where forest fires occured in spring and soils are uncovered by vegetation (which is the case especially for Ticino) (Marxer, 2003). The combination of the monthly rainfall erosivity maps with dynamic monthly C-factors might enable a monthly soil erosion

30   risk assessment for Switzerland.

3.5 Monthly erosivity density

Erosivity density (expressed as ratios of R to P) can be used to distinguish between high rainfall erosivity which is mainly influenced by high rainfall amounts and those which is influenced by relatively low rainfall amounts but highly intense rainfalls. That distinction helps to evaluate the potential consequences of rainfall erosivity for each month. The ED_{mo} maps (Fig. 7) show that the influence of rainfall intensity on rainfall erosivity also underlies seasonal and spatial variations. Interpolated and spatially averaged ED_{mo} in winter is lower than 1 MJ ha^{-1} h^{-1} (Fig. 7) for Switzerland. Therefore, rainfall intensity is not the driving factor for rainfall erosivity in these months where low rainfall erosivity meets high rainfall amounts. The relative high R_{mo} in the Jura Mountains is therefore mainly driven by large amounts of rainfall instead of high intensity rains. Interpolated and spatially averaged ED_{mo} has a maximum for Switzerland in July (1.8 MJ ha^{-1} h^{-1}) which results from a relatively low rainfall amount indicating that rainfall erosivity is mainly controlled by high intensified events. Intense summer rainfall has its maximum in the regions of Jura, Swiss Midland, northern Alpine foothill, and Southern Alps. In these regions, R_{mo} is high accompanied by relative low precipitation amounts. As such, the erosivity risk is the highest within the year especially when soils are dry during periods of rare but high rainfall intensities and therefore, infiltration is reduced due to crusts.

The distribution of the Swiss mean ED_{mo} (Fig. 8) is bell-shaped as it is also the case for investigated stations in the United States, Italy and Austria (Foster et al., 2008; Dabney et al., 2012; Borrelli et al., 2016; Panagos et al., 2016a). The monthly erosivity density of the neighbouring country Austria complies with the Swiss values only with minor variability. Greece, Italy and the stations of the US are characterized by higher ED_{mo} values than Switzerland. Nonetheless, the conclusion Panagos et al. (2016b) drew for Greece that "rainfall erosivity is not solely dependent on the amount of precipitation" is also generally valid for Switzerland.

In addition to the ED_{mo}-maps, ED_{mo87} at the 87 stations (Table S1) were calculated. ED_{mo87} show generally higher values than ED_{mo} calculated from the interpolated raster maps, since the interpolated R-factors are smoothed and adapted according to the surrounding values. This fact is also visible in Fig. S2, where the relationship of absolute R-factors at the 87 stations (R_{mo87}) and the interpolated R-factors at the 87 stations (extracted after the interpolation with Regression-Kriging; $R_{Regression-Kriging}$) is presented.

4 Conclusion and Outlook

The main aim of the current study was to investigate the seasonal and regional variability of rainfall erosivity in Switzerland. A crucial advancement of the present research was to identify spatial and temporal windows of high erosivity. Through the spatial-temporal mapping, it was possible to determine regions that are hardly affected by rainfall erosivity, such as Grisons and Wallis, and it was also possible to determine those that are only affected in a certain months, such as Jura Mountains. The spatio-temporal variability of rainfall erosivity of Switzerland enables the controlled and time-dependent management of agriculture (like crop selection, time-dependent sowing) and droughts, ecosystem services evaluation, as well as the use for

seasonal and regional hazard prediction (e.g. flood risk control, landslide susceptibility mapping). Rainfall erosivity based on high erosivity density has more severe impacts on soils, agriculture, droughts, and hazards in summer than in winter due the high impact of intense rainfalls.

In contrast to previous studies for Switzerland which were either limited spatially (to a few stations) or temporally (to annual) we were able to produce 12 monthly spatio-temporal R-factor maps. The maps are based on high resolution covariates in combination with an extended database of 87 automated gauging-stations recording in 10 min intervals, showing simultaneously spatial and temporal variations of R-factors. Regression-Kriging based on high resolution covariates was a successful method for most of the months (mean R^2=0.51, E_{RMS}=93.27 MJ mm ha^{-1} h^{-1} $month^{-1}$). It was used to map the long-term monthly mean R-factors based on an extended database of rain-gauging stations. The spatio-temporal mapping of rainfall erosivity and erosivity density revealed that intense rainfall events in August trigger the highest national monthly mean rainfall erosivity value (263.5 MJ mm ha^{-1} h^{-1} $month^{-1}$). Especially the regions of Jura, Swiss Midland, northern Alpine foothill, and Ticino at the Southern Alps show pronounced rainfall erosivity during that month. The months June to September have a total share of 62% of the total annual rainfall erosivity in Switzerland.

The current data highlight that rainfall erosivity has a very high variability within a year. These trends of seasonality vary between regions and consequently support that a dynamic soil erosion and natural hazard risk assessment is crucial. The combination of the temporally varying RUSLE-factors (R- and C-factor) will lead to a more realistic and time-dependent estimation of soil erosion within a year which is valuable for the identification of more susceptible seasons and regions. A mapping of the seasonality of the C-factor for a subsequent synthesis to a dynamic soil erosion risk assessment for Switzerland is envisaged in a later study.

The findings of this study have a number of important implications for soil conservation planning. Based on the knowledge of the variability of rainfall erosivity, agronomists can introduce selective erosion control measures, a change in crop or crop rotation to weaken of the rainfalls impact on soils and vegetation by increasing soil cover or stabilizing topsoil during these susceptible months. As such, a targeted erosion control for Switzerland does not only reduce the direct costs of erosion by mitigation but also shrinks the costs for the implementation of control measures to a requested minimum.

Author contribution

S. Schmidt, K. Meusburger and C. Alewell analysed the data; S. Schmidt, K. Meusburger, C. Alewell, and P. Panagos wrote the paper.

Acknowledgement

The research has been funded by the Swiss Federal Office for the Environment (FOEN) (project N° N222-0350). We would like to thank MeteoSwiss, SwissTopo, and the cantons Lucerne, Berne, and St. Gallen for providing the datasets.

Conflict of interest

The authors confirm and sign that there is no conflict of interest with networks, organizations and data centers referred to in the paper.

References

Agnese, C., Bagarello, V., Corrao, C., D'Agostino, L., and D'Asaro, F.: Influence of the rainfall measurement interval on the erosivity determinations in the Mediterranean area, Journal of Hydrology, 329, 39–48, doi:10.1016/j.jhydrol.2006.02.002, 2006.

Alewell, C., Meusburger, K., Juretzko, G., Mabit, L., and Ketterer, M. E.: Suitability of 239+240Pu and 137Cs as tracers for soil erosion assessment in mountain grasslands, Chemosphere, 103, 274–280, doi:10.1016/j.chemosphere.2013.12.016, 2014.

Angulo-Martínez, M. and Beguería, S.: Estimating rainfall erosivity from daily precipitation records: A comparison among methods using data from the Ebro Basin (NE Spain), Journal of Hydrology, 379, 111–121, doi:10.1016/j.jhydrol.2009.09.051, 2009

Arnhold, S., Lindner, S., Lee, B., Martin, E., Kettering, J., Nguyen, T. T., Koellner, T., Ok, Y. S., and Huwe, B.: Conventional and organic farming: Soil erosion and conservation potential for row crop cultivation, Geoderma, 219-220, 89–105, doi:10.1016/j.geoderma.2013.12.023, 2014.

Banasik, K. and Górski, D.: Evaluation of Rainfall Erosivity for East Poland, Proceedings of the Warsaw Symposium, 1993.

Banasik, K., Górski, D., and Mitchell, J. K.: Rainall Erosivity for East and Central Poland, International Symposium on Soil Erosion Research for the 21st Century, 279–282, 2001.

Begert, M., Schlegel, T., and Kirchhofer, W.: Homogeneous temperature and precipitation series of Switzerland from 1864 to 2000, International Journal of Climatology, 25, 65–80, doi:10.1002/joc.1118, 2005.

Bonilla, C. and Vidal, K.: Rainfall erosivity in Central Chile, Journal of Hydrology, 410, 126–133, doi:10.1016/j.jhydrol.2011.09.022, 2011.

Borrelli, P., Diodato, N., and Panagos, P.: Rainfall erosivity in Italy: A national scale spatio-temporal assessment, International Journal of Digital Earth, 1–16, doi:10.1080/17538947.2016.1148203, 2016.

Brown, L. and Foster, G.: Storm Erosivity Using Idealized Intensity Distributions, Transactions of the ASAE, 30, 379–386, doi:10.13031/2013.31957, 1987.

da Silva, A. M.: Rainfall erosivity map for Brazil, CATENA, 57, 251–259, doi:10.1016/j.catena.2003.11.006, 2004.

da Silva, A. M., Wiecheteck, M., and Zuercher, B. W.: Spatial Assessment of Indices for Characterizing the Erosive Force of Rainfall in El Salvador Republic, Environmental Engineering Science, 28, 309–316, doi:10.1089/ees.2010.0296, 2011.

da Silva, R. M., Santos, C. A. G., de Lima Silva, Valeriano Carneiro, and e Silva, L. P.: Erosivity, surface runoff, and soil erosion estimation using GIS-coupled runoff–erosion model in the Mamuaba catchment, Brazil, Environ Monit Assess, 185, 8977–8990, doi:10.1007/s10661-013-3228-x, 2013.

Dabney, S. M., Yoder, D. C., Vieira, D., and Bingner, R. L.: Enhancing RUSLE to include runoff-driven phenomena, Hydrol. Process., 25, 1373–1390, doi:10.1002/hyp.7897, 2011.

Dabney, S. M., Yoder, D. C., and Vieira, D. A. N.: The application of the Revised Universal Soil Loss Equation, Version 2, to evaluate the impacts of alternative climate change scenarios on runoff and sediment yield, Journal of Soil and Water Conservation, 67, 343–353, doi:10.2489/jswc.67.5.343, 2012.

Davison, P., Hutchins, M. G., Anthony, S. G., Betson, M., Johnson, C., and Lord, E. I.: The relationship between potentially erosive storm energy and daily rainfall quantity in England and Wales, The Science of the total environment, 344, 15–25, doi:10.1016/j.scitotenv.2005.02.002, 2005.

Diodato, N.: Predicting RUSLE (Revised Universal Soil Loss Equation) Monthly Erosivity Index from Readily Available Rainfall Data in Mediterranean Area, Environmentalist, 26, 63–70, doi:10.1007/s10669-006-5359-x, 2005.

Efron, B. and Tibshirani, R.: Improvements on Cross-Validation: The .632+ Bootstrap Method, Journal of the American Statistical Association, 92, 548, doi:10.2307/2965703, 1997.

Foster, G. R., Yoder, D. C., Weesies, G. A., McCool, D. K., McGregor, K. C., and Bingner, R.: Draft User's Guide, Revised Universal Soil Loss Equation Version 2 (RUSLE-2), Washington, DC, 2008.

Friedli, S.: Digitale Bodenerosionsgefährdungskarte Der Schweiz Im Hektarraster – Unter Besonderer Berücksichtigung des Ackerlandes, Bern, 2006.

Fuhrer, J., Beniston, M., Fischlin, A., Frei, C., Goyette, S., Jasper, K., and Pfister, C.: Climate Risks and Their Impact on Agriculture and Forests in Switzerland, Climatic Change, 79, 79–102, doi:10.1007/s10584-006-9106-6, 2006.

Gisler, S., Lininger, H.-P., and Prasuhn, V.: Erosionsrisikokarte im 2x2-Meter-Raster (ERK2), Agrarforschung Schweiz, 2, 2011.

Gotway, C. A. and Stroup, W. W.: A Generalized Linear Model Approach to Spatial Data Analysis and Prediction, Journal of Agricultural, Biological, and Environmental Statistics, 2, 157–178, 1997.

Gupta, B. C. and Guttman, I.: Statistics and probability with applications for engineers and scientists, John Wiley & Sons Inc, Hoboken, New Jersey, 876 pp., 2013.

Hanel, M., Máca, P., Bašta, P., Vlnas, R., and Pech, P.: Rainfall erosivity factor in the Czech Republic and its Uncertainty, Hydrol. Earth Syst. Sci. Discuss., 1–24, doi:10.5194/hess-2016-158, 2016.

Harrell Jr., F.: Regression Modeling Strategies: With Applications to Linear Models, Logistic and Ordinal Regression, and Survival Analysis, Cham, 2015.

5 Hartwig, N. L. and Ammon, H. U.: Cover crops and living mulches, Weed Science, 50, 688–699, doi:10.1614/0043-1745(2002)050[0688:AIACCA]2.0.CO;2, 2002.

Hengl, T., Heuvelink, G., and Rossiter, D.: About regression-kriging: From equations to case studies, Computers & Geosciences, 33, 1301–1315, doi:10.1016/j.cageo.2007.05.001, 2007.

Hengl, T., Heuvelink, G., and Stein, A.: A generic framework for spatial prediction of soil variables based on regression-10 kriging, Geoderma, 120, 75–93, doi:10.1016/j.geoderma.2003.08.018, 2004.

Hengl, T.: A practical guide to geostatistical mapping of environmental variables, EUR, 22904EN, Publications Office, Luxembourg, 2007.

Hollinger, S. E., Angel, J. R., and Palecki, M. A.: Spatial Distribution, Variation, an Trends in Storm Precipitation Characteristics Associated with Soil Erosion in the United States, Champaign, 2002.

15 Hurni, H.: Bestimmung der Erosivität von Hagelereignissen: Empirische Bestimmung der Erosivität von Hagelereignissen, Unpublished manuscript, 1978.

Isotta, F., Frei, C., Weilguni, V., Perčec T., M., Lassègues, P., Rudolf, B., Pavan, V., Cacciamani, C., Antolini, G., Ratto, S., Munari, M., Micheletti, S., Bonati, V., Lussana, C., Ronchi, C., Panettieri, E., Marigo, G., and Vertačnik, G.: The climate of daily precipitation in the Alps: Development and analysis of a high-resolution grid dataset from pan-Alpine rain-gauge data, 20 International Journal of Climatology), 34, 1657–1675, doi:10.1002/joc.3794, 2014.

James, G. and Witten, D.: An introduction to statistical learning: With applications in R, Corr. at 6. printing, Springer texts in statistics, Springer, New York, NY, 426 pp., 2015.

Jing, Z., Xu-dong, Z., Jin-xing, Z., Xiao-ling, Z., and Zhong-jian, W.: Calculation and Characterization of Rainfall Erosivity in Small Watersheds of Hilly Region in Northwest Hunan (in chinese), Journal of Ecology and Rural Environment, 25, 32–25 36, 2009.

Klik, A., Haas, K., Dvorackova, A., and Fuller, I. C.: Spatial and temporal distribution of rainfall erosivity in New Zealand, Soil Res., 53, 815, doi:10.1071/SR14363, 2015.

Konz, N., Prasuhn, V., and Alewell, C.: On the measurement of alpine soil erosion, CATENA, 91, 63–71, doi:10.1016/j.catena.2011.09.010, 2012.

Köppen, W.: Das geographische System der Klimate, Handbuch der Klimatologie, 1, Berlin, 1936.

Kutner, M. H., Nachtsheim, C., Neter, J., and Li, W.: Applied linear statistical models, 5. ed., McGraw-Hill/Irwin series Operations and decision sciences, Boston, 1396 pp., 2005.

Laceby, J. P., Chartin, C., Evrard, O., Onda, Y., Garcia-Sanchez, L., and Cerdan, O.: Rainfall erosivity in subtropical
5 catchments and implications for erosion and particle-bound contaminant transfer: A case-study of the Fukushima region, Hydrol. Earth Syst. Sci. Discuss., 12, 7225–7266, doi:10.5194/hessd-12-7225-2015, 2015.

Lai, C., Xiaohong, C., Zhaoli, W., Xushu, W., Shiwei, Z., Xiaoqing, W., and Wenkui, B.: Spatio-temporal variation in rainfall erosivity during 1960–2012 in the Pearl River Basin, China, CATENA, 137, 382–391, doi:10.1016/j.catena.2015.10.008, 2016.

10 Ledermann, T.: Multiple Implications of Soil Erosion and Conservation on Arable Farm Land in the Swiss Midlands, Bern, 2012.

Lee, J. S. and Won, J. Y.: Analysis of the Characteristic of Monthly Rainfall Erosivity in Korea with Derivation of Rainfall Energy Equation, Journal of korean society of hazard mitigation, 13, 177–184, doi:10.9798/KOSHAM.2013.13.3.177, 2013.

Leek, R. and Olsen, P.: Modelling climatic erosivity as a factor for soil erosion in Denmark: Changes and temporal trends,
15 Soil Use and Management, 16, 61–65, doi:10.1111/j.1475-2743.2000.tb00175.x, 2000.

Ma, X., He, Y., Xu, J., van Noordwijk, M., and Lu, X.: Spatial and temporal variation in rainfall erosivity in a Himalayan watershed, CATENA, 121, 248–259, doi:10.1016/j.catena.2014.05.017, 2014.

Mannaerts, C. and Gabriels, D.: Rainfall erosivity in Cape Verde, Soil and Tillage Research, 55, 207–212, doi:10.1016/S0167-1987(00)00104-5, 2000.

20 Marxer, P.: Oberflächenabfluß und Bodenerosion auf Brandflächen des Kastanienwaldgürtels der Südschweiz mit einer Anleitung zur Bewertung der post-fire Erosionsanfälligkeit (BA EroKaBr), Physiogeographica, 33, Wepf in Komm, Basel, 2003.

McBratney, A. B., Odeh, I. O., Bishop, T. F., Dunbar, M. S., and Shatar, T. M.: An overview of pedometric techniques for use in soil survey, Geoderma, 97, 293–327, doi:10.1016/S0016-7061(00)00043-4, 2000.

25 Meshesha, D., Tsunekawa, A., Tsubo, M., Haregeweyn, N., and Adgo, E.: Evaluating spatial and temporal variations of rainfall erosivity, case of Central Rift Valley of Ethiopia, Theor Appl Climatol, 119, 515–522, doi:10.1007/s00704-014-1130-2, 2015.

MeteoSwiss: Documentation of MeteoSwiss Grid-Data Products: Monthly and Yearly Precipitation: RhiresM and RhiresY, Zürich, 2013.

Meusburger, K. and Alewell, C.: Impacts of anthropogenic and environmental factors on the occurrence of shallow landslides in an alpine catchment (Urseren Valley, Switzerland), Nat. Hazards Earth Syst. Sci., 8, 509–520, doi:10.5194/nhess-8-509-2008, 2008.

Meusburger, K., Steel, A., Panagos, P., Montanarella, L., and Alewell, C.: Spatial and temporal variability of rainfall erosivity factor for Switzerland, Hydrol. Earth Syst. Sci., 16, 167–177, doi:10.5194/hess-16-167-2012, 2012.

Mikoš, M., Jošt, D., and Petkovšek, G.: Rainfall and runoff erosivity in the alpine climate of north Slovenia: A comparison of different estimation methods, Hydrological Sciences Journal, 51, 115–126, doi:10.1623/hysj.51.1.115, 2006.

Mosimann, T., Crole-Rees, A., Maillard, A., Neyroud, J.-A., Thöni, M., Musy, A., and Rohr, W.: Bodenerosion im Schweizerischen Mittelland: Ausmass und Gegenmassnahmen, Bericht 51 des Nationalen Forschungsprogrammes Nutzung des Bodens in der Schweiz, Liebefeld-Bern, 1990.

Mosimann, T., Maillard, A., Musy, A., Neyroud, J.-A., Rüttimann, M., and Weisskopf, P.: Erosionsbekämpfung in Ackerbaugebieten: Ein Leitfaden für die Bodenerhaltung, Themenbericht des NAtionalen Forschungsprogrammes "Nutzung des Bodes in der Schweiz", 1991.

Nisi, L., Martius, O., Hering, A., Kunz, M., and Germann, U.: Spatial and temporal distribution of hailstorms in the Alpine region: A long-term, high resolution, radar-based analysis, Q.J.R. Meteorol. Soc., doi:10.1002/qj.2771, 2016.

Nogler, S.: Erosvität der Niederschläge im schweizerischen Mittelland, Bern, 2012.

Odeh, I., McBratney, A. B., and Chittleborough, D. J.: Further results on prediction of soil properties from terrain attributes: Heterotopic cokriging and regression-kriging, Geoderma, 67, 215–226, doi:10.1016/0016-7061(95)00007-B, 1995.

Özşahin, E.: An assessment of monthly rainfall erosivity model for Amik Plain (Hatay, S TURKEY), Photon, 177–193, 2014.

Panagos, P., Ballabio, C., Borrelli, P., and Meusburger, K.: Spatio-temporal analysis of rainfall erosivity and erosivity density in Greece, CATENA, 137, 161–172, doi:10.1016/j.catena.2015.09.015, 2016b.

Panagos, P., Ballabio, C., Borrelli, P., Meusburger, K., Klik, A., Rousseva, S., Tadić, M., Michaelides, S., Hrabalíková, M., Olsen, P., Aalto, J., Lakatos, M., Rymszewicz, A., Dumitrescu, A., Beguería, S., and Alewell, C.: Rainfall erosivity in Europe, The Science of the total environment, 511, 801–814, doi:10.1016/j.scitotenv.2015.01.008, 2015.

Panagos, P., Borrelli, P., Spinoni, J., Ballabio, C., Meusburger, K., Beguería, S., Klik, A., Michaelides, S., Petan, S., Hrabalíková, M., Olsen, P., Aalto, J., Lakatos, M., Rymszewicz, A., Dumitrescu, A., Perčec Tadić, M., Diodato, N., Kostalova, J., Rousseva, S., Banasik, K., and Alewell, C.: Monthly Rainfall Erosivity: Conversion Factors for Different Time Resolutions and Regional Assessments, Water, 8, 119, doi:10.3390/w8040119, 2016a.

Petkovšek, G. and Mikoš, M.: Estimating the R factor from daily rainfall data in the sub-Mediterranean climate of southwest Slovenia / Estimation du facteur R à partir de données journalières de pluie dans le climat sub-méditerranéen du Sud-Ouest de la Slovénie, Hydrological Sciences Journal, 49, doi:10.1623/hysj.49.5.869.55134, 2004.

Perroud, M. and Bader, S.: Klimaänderung in der Schweiz. Indikatoren zu Ursachen, Auswirkungen, Massnahmen., Umwelt-Zustand, 2013.

Porto, P.: Exploring the effect of different time resolutions to calculate the rainfall erosivity factor R in Calabria, southern Italy, Hydrol. Process., 30, 1551–1562, doi:10.1002/hyp.10737, 2016.

Prasuhn, V.: Soil erosion in the Swiss midlands: Results of a 10-year field survey, Geomorphology, 126, 32–41, doi:10.1016/j.geomorph.2010.10.023, 2011.

Prasuhn, V.: On-farm effects of tillage and crops on soil erosion measured over 10 years in Switzerland, Soil and Tillage Research, 120, 137–146, doi:10.1016/j.still.2012.01.002, 2012.

Prasuhn, V., Liniger, H., Gisler, S., Herweg, K., Candinas, A., and Clément, J.-P.: A high-resolution soil erosion risk map of Switzerland as strategic policy support system, Land Use Policy, 32, 281–291, doi:10.1016/j.landusepol.2012.11.006, 2013.

Punge, H. J. and Kunz, M.: Hail observations and hailstorm characteristics in Europe: A review, Atmospheric Research, 176-177, 159–184, doi:10.1016/j.atmosres.2016.02.012, 2016.

Renard, K. G., Foster, G., Weesies, G., McCool, D. K., and Yoder, D. C.: Prediction Soil Erosion by Water: A Guide to Conservation Planning with the Revised Universal Soil Loss Equation (RUSLE), Agriculture handbook, 703, 1997.

Renschler, C. S., Mannaerts, C., and Diekkrüger, B.: Evaluating spatial and temporal variability in soil erosion risk—rainfall erosivity and soil loss ratios in Andalusia, Spain, CATENA, 34, 209–225, doi:10.1016/S0341-8162(98)00117-9, 1999.

Sadeghi, S., Moatamednia, M., and Behzadfar, M.: Spatial and Temporal Variations in the Rainfall Erosivity Factor in Iran, J. Agr. Sci. Tech., 451–464, 2011.

Sadeghi, S. H. R. and Hazbavi, Z.: Trend analysis of the rainfall erosivity index at different time scales in Iran, Nat Hazards, 77, 383–404, doi:10.1007/s11069-015-1607-z, 2015.

Sadeghi, S. H. and Tavangar, S.: Development of stational models for estimation of rainfall erosivity factor in different timescales, Nat Hazards, 77, 429–443, doi:10.1007/s11069-015-1608-y, 2015.

Sanchez-Moreno, J. F., Mannaerts, C. M., and Jetten, V.: Rainfall erosivity mapping for Santiago Island, Cape Verde, Geoderma, 217-218, 74–82, doi:10.1016/j.geoderma.2013.10.026, 2014.

Schwarb, M., Daly, C., Frei, C., and Schär, C.: Mean Seasonal Precipitation throughout the European Alps 1971-1990, in: Hydrological Atlas of Switzerland, Wingartner, R. (Ed.), Bern, 2001.

Schwertmann, U., Vogl, W., and Kainz, M.: Bodenerosion durch Wasser: Vorhersage des Abtrags und Bewertung von Gegenmaßnahmen, Stuttgart, 64 pp., 1987.

Shamshad, A., Azhari, M. N., Isa, M. H., Hussin, W. W., and Parida, B. P.: Development of an appropriate procedure for estimation of RUSLE EI30 index and preparation of erosivity maps for Pulau Penang in Peninsular Malaysia, CATENA, 72, 423–432, doi:10.1016/j.catena.2007.08.002, 2008.

Sideris, I., Gabella, M., and Germann, U.: The CombiPrecip experience: development and operation of a real-time radar-raingauge combination scheme in Switzerland, 2014 International Weather Radar and Hydrology Symposium (Ed.), 2014.

Spreafico, M. and Weingartner, R.: Hydrologie der Schweiz: Ausgewählte Aspekte und Resultate, Berichte des BWG, Serie Wasser, 2005.

Steyerberg, E.: Clinical Prediction Models: A Practical Approach to Development, Validation, and Updating, New York, NY, 2009.

Terranova, O. G. and Gariano, S. L.: Regional investigation on seasonality of erosivity in the Mediterranean environment, Environ Earth Sci, 73, 311–324, doi:10.1007/s12665-014-3426-z, 2015.

Torriani, D. S., Calanca, P., Schmid, S., Beniston, M., and Fuhrer, J.: Potential effects of changes in mean climate and climate variability on the yield of winter and spring crops in Switzerland, Clim. Res., 34, 59–69, doi:10.3354/cr034059, 2007.

van Delden, A.: The synoptic setting of thunderstorms in western Europe, Atmospheric Research, 56, 89–110, doi:10.1016/S0169-8095(00)00092-2, 2001.

Verstraeten, G., Poesen, J., Demarée, G., and Salles, C.: Long-term (105 years) variability in rain erosivity as derived from 10-min rainfall depth data for Ukkel (Brussels, Belgium): Implications for assessing soil erosion rates, J. Geophys. Res., 111, doi:10.1029/2006JD007169, 2006.

Vrieling, A., Hoedjes, J. C., and van der Velde, M.: Towards large-scale monitoring of soil erosion in Africa: Accounting for the dynamics of rainfall erosivity, Global and Planetary Change, 115, 33–43, doi:10.1016/j.gloplacha.2014.01.009, 2014.

Wang, L. L., Yang, E., Huang, J., and Jiao, P.: Spatial and Temporal Characteristics of Rainfall Erosivity of Shanghai in Recent Ten Years, AMM, 295-298, 2084–2089, doi:10.4028/www.scientific.net/AMM.295-298.2084, 2013.

Weisshaidinger, R. and Leser, H.: Switzerland, in: Soil erosion in Europe, Boardman, J., Poesen, J. (Eds.), Wiley-Interscience, Hoboken, NJ, 2006.

Wellinger, R., Buser, H.-P., Krauss, J., and Theiler, R.: Karotten: Anbau, Erntezeitpunkt und Lagerung, Agrarforschung Schweiz, 13, 412–417, 2006.

Wilkes, G. and Sawada, M.: Geostatistically Derived Great Lakes USLE Monthly Rainfall Erosivity Factors, Journal of Great Lakes Research, 31, 155–165, doi:10.1016/S0380-1330(05)70247-1, 2005.

Wischmeier, W. H. and Smith, D. D.: Predicting rainfall erosion losses, Agriculture handbook, 537, U.S. Gov. Print. Off, Washington, 58 pp., 1978.

5 Yang, X. and Yu, B.: Modelling and mapping rainfall erosivity in New South Wales, Australia, Soil Res., doi:10.1071/SR14188, 2015.

Yang, X., Yu, B., and Zhu, Q.: Climate change impacts on rainfall erosivity and hillslope erosion in NSW, 21st International congress on Modelling and Simulation, Gold Coarst, Australia, 2015.

Zhao, Q., Liu, Q., Ma, L., Ding, S., Xu, S., W., C., and Liu, P.: Spatiotemporal variations in rainfall erosivity during the
10 period of 1960–2011 in Guangdong Province, southern China, Theor Appl Climatol, doi:10.1007/s00704-015-1694-5, 2015.

Zhu, Q., Chen, X., Fan, Q., Jin, H., and Li, J.: A new procedure to estimate the rainfall erosivity factor based on Tropical Rainfall Measuring Mission (TRMM) data, Sci. China Technol. Sci., 54, 2437–2445, doi:10.1007/s11431-011-4468-z, 2011.

Tables

Table 1: Datasets used as covariates for the spatio-temporal mapping of rainfall erosivity.

dataset	derived information	temporal resolution	spatial resolution	measuring period	source	information
Total snow depth	long-term monthly snow depth	hourly	58 stations	1988 – 2010	MeteoSwiss	-
CombiPrecip	long-term monthly mean rainfall amount from measured and radar data	hourly	1 km	2005 – 2015	MeteoSwiss	Sideris et al., 2014
EURO4M-APGD	long-term mean daily precipitation per month	monthly	5 km	1971 – 2008	MeteoSwiss	Isotta et al., 2014
RhiresM	long-term mean monthly precipitation sums	monthly	1 km	1961 – 2015	MeteoSwiss	MeteoSwiss, 2013
SwissAlti3D	elevation, slope, aspect	-	2 m	-	SwissTopo	-

Table 2: Regression equations and selected covariates for estimating mean monthly rainfall erosivity in Switzerland.

Month	Regression equation
January	$R_{Jan} = 2.101 - 4.150 \cdot CombiPrecip_{Jan} - 0.006 \cdot Snow\ depth_{Jan} + 0.017 \cdot Rhires_{Jan} - 0.001 \cdot Elevation$
February	$R_{Feb} = 2.702 - 13.812 \cdot CombiPrecip_{Feb} - 0.007 \cdot Snow\ depth_{Feb} + 0.019 \cdot Rhires_{Feb} + 0.211 \cdot Alpine\ Precip_{Feb} - 0.001 \cdot Elevation$
March	$R_{Mar} = 2.534 - 7.735 \cdot CombiPrecip_{Mar} - 0.006 \cdot Snow\ depth_{Mar} + 0.018 \cdot Rhires_{Mar} + 0.170 \cdot Alpine\ Precip_{Mar} - 0.001 \cdot Elevation$
April	$R_{Apr} = 2.330 - 3.319 \cdot CombiPrecip_{Apr} - 0.008 \cdot Snow\ depth_{Apr} + 0.023 \cdot Rhires_{Apr} - 0.001 \cdot Elevation - 0.019 \cdot Slope$
May	$R_{May} = 2.965 + 2.072 \cdot CombiPrecip_{May} - 0.002 \cdot Snow\ depth_{May} + 0.015 \cdot Rhires_{May} - 0.001 \cdot Elevation$
June	$R_{Jun} = 3.890 + 0.014 \cdot Rhires_{Jun} - 0.001 \cdot Elevation$
July	$R_{Jul} = 3.926 + 5.710 \cdot CombiPrecip_{Jul} + 0.251 \cdot Alpine\ Precip_{Jul} - 0.001 \cdot Elevation$
August	$R_{Aug} = 3.627 + 0.010 \cdot Rhires_{Aug} + 0.194 \cdot Alpine\ Precip_{Aug} - 0.001 \cdot Elevation$
September	$R_{Sep} = 2.760 + 2.243 \cdot CombiPrecip_{Sep} + 0.539 \cdot Alpine\ Precip_{Sepb} - 0.001 \cdot Elevation$
October	$R_{Oct} = 2.753 + 0.0161 \cdot Rhires_{Oct} - 0.001 \cdot Elevation$
November	$R_{Nov} = 2.665 + 3.787 \cdot CombiPrecip_{Nov} - 0.034 \cdot Snow\ depth_{Nov} + 0.166 \cdot Alpine\ Precip_{Nov}$
December	$R_{Dec} = 2.437 + 0.013 \cdot Rhires_{Dec} - 0.001 \cdot Elevation$

Table 3: Model efficiency by R² and E$_{RMS}$ as well as omitted outliers and influential observations per month.

Month	Excl. outlier stations	R²	E$_{RMS}$ (MJ mm ha^{-1} h^{-1} month^{-1})	Null Deviance	Res. deviance
January	Mathod	0.52	6.98	70.36	20.65
February	Monte Generoso, Napf, Saetis	0.53	12.96	79.28	31.82
March	Col du Grand St-Bernard, Saetis	0.49	13.10	61.45	21.84
April	Col du Grand St-Bernard, Saetis, Weissfluhjoch	0.65	21.01	63.69	15.90
May	Davos, Col du Grand St-Bernard	0.60	73.39	56.28	16.83
June	Col du Grand St-Bernard	0.58	126.03	51.61	19.31
July	Monte Generoso, Col du Grand St-Bernard, Stabio	0.66	138.77	38.58	11.57
August	Col du Grand St-Bernard, Stabio	0.47	330.16	50.47	21.75
September	Col du Grand St-Bernard, Stabio	0.64	81.91	61.23	16.27
October	Piz Corvatsch, Col du Grand St-Bernard, Stabio	0.62	81.60	37.86	12.07
November	Piz Corvatsch, Col du Grand St-Bernard, Saetis	0.10	55.72	58.85	47.22
December	Col du Grand St-Bernard	0.26	177.65	73.90	50.66

Table 4: Monthly national rainfall erosivity in MJ mm ha^{-1} h^{-1} month^{-1}.

Month	Minima	Maxima	Mean
January	0.2	71.3	10.5
February	0.0	247.3	13.5
March	0.0	179.0	20.1
April	0.2	1014.4	28.8
May	8.3	1717.8	120.2
June	3.6	1262.1	174.8
July	12.6	1481.1	255.4
August	8.3	1994.9	263.5
September	6.8	6107.9	147.7
October	5.7	977.0	57.0
November	4.9	357.1	41.6
December	1.3	234.4	24.9

Figures
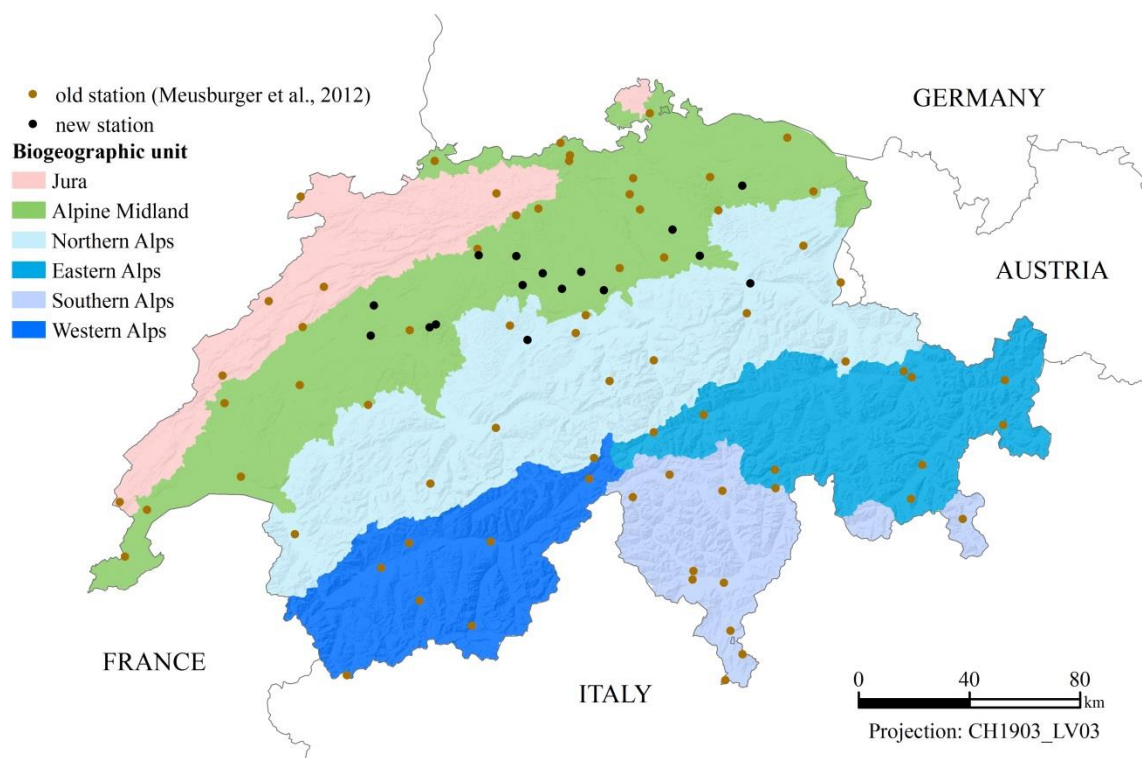
Figure 1: Biogeographic units and used gauging stations in Switzerland.
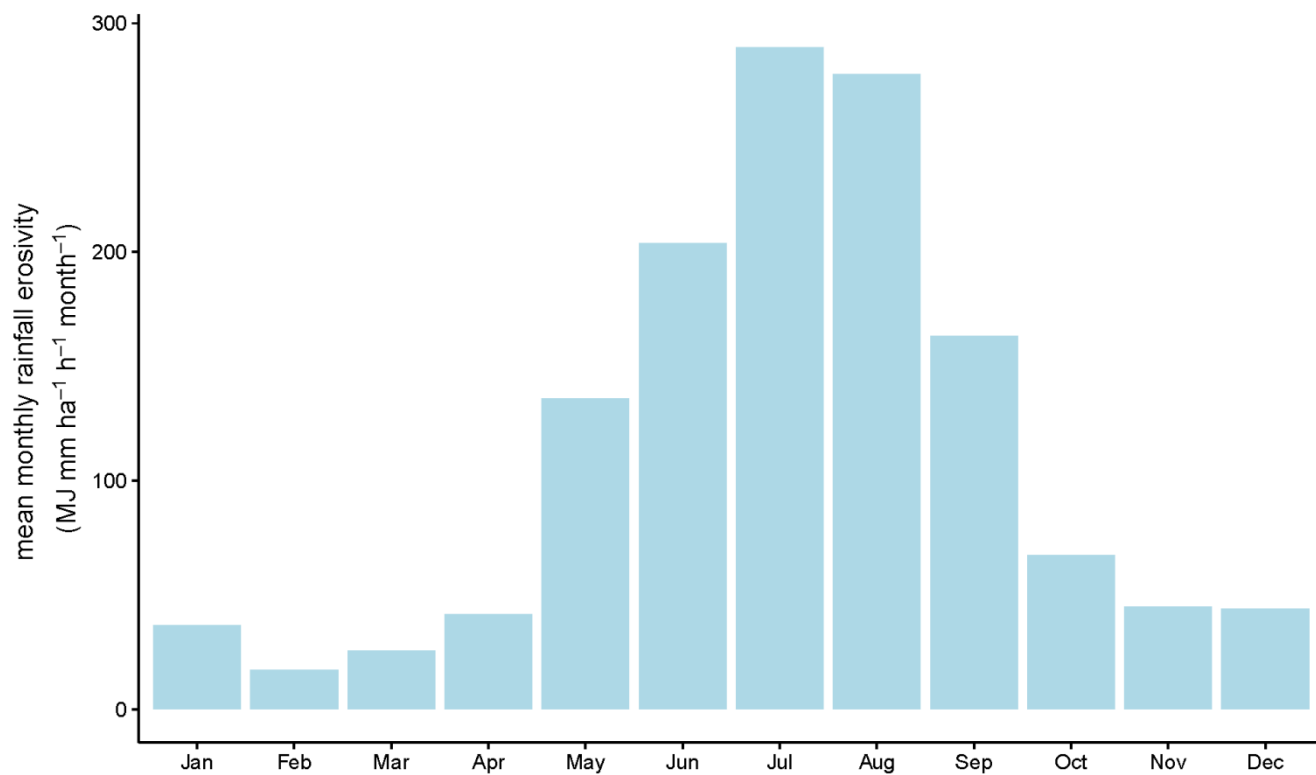
Figure 2: Mean monthly rainfall erosivity for all 87 Swiss stations.
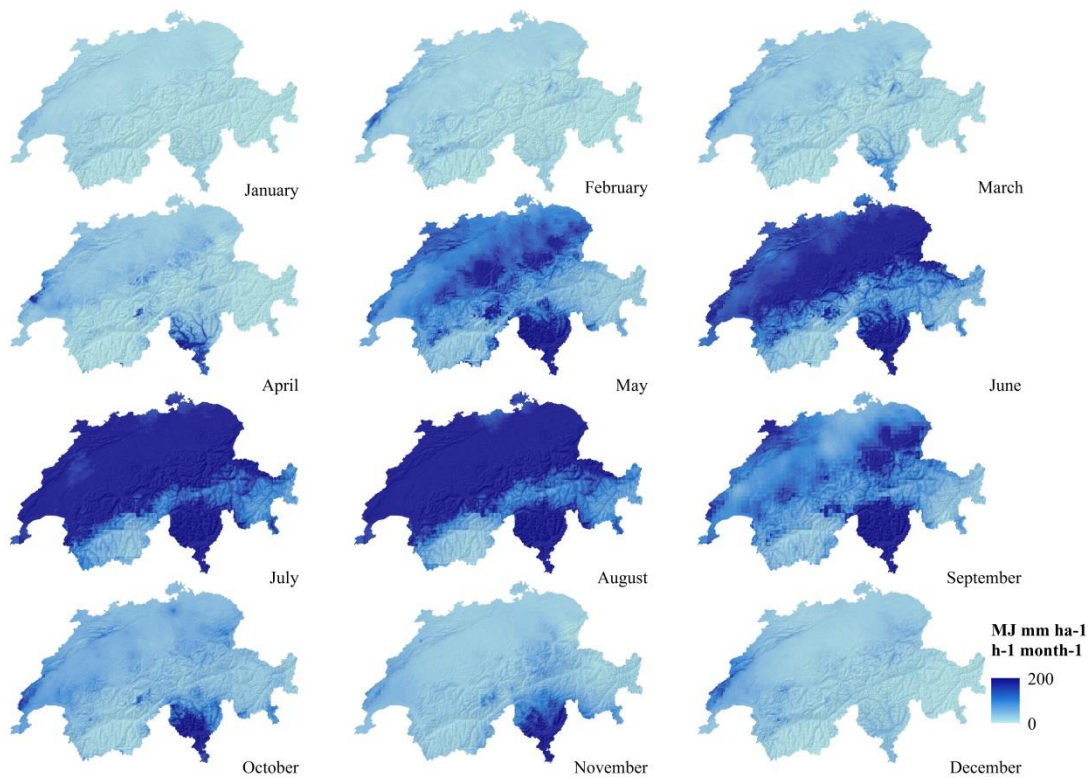
Figure 3: Monthly rainfall erosivity maps for Switzerland (equal stretch from 0 to 200 MJ mm ha^{-1} h^{-1} month^{-1}) derived by regression-kriging.
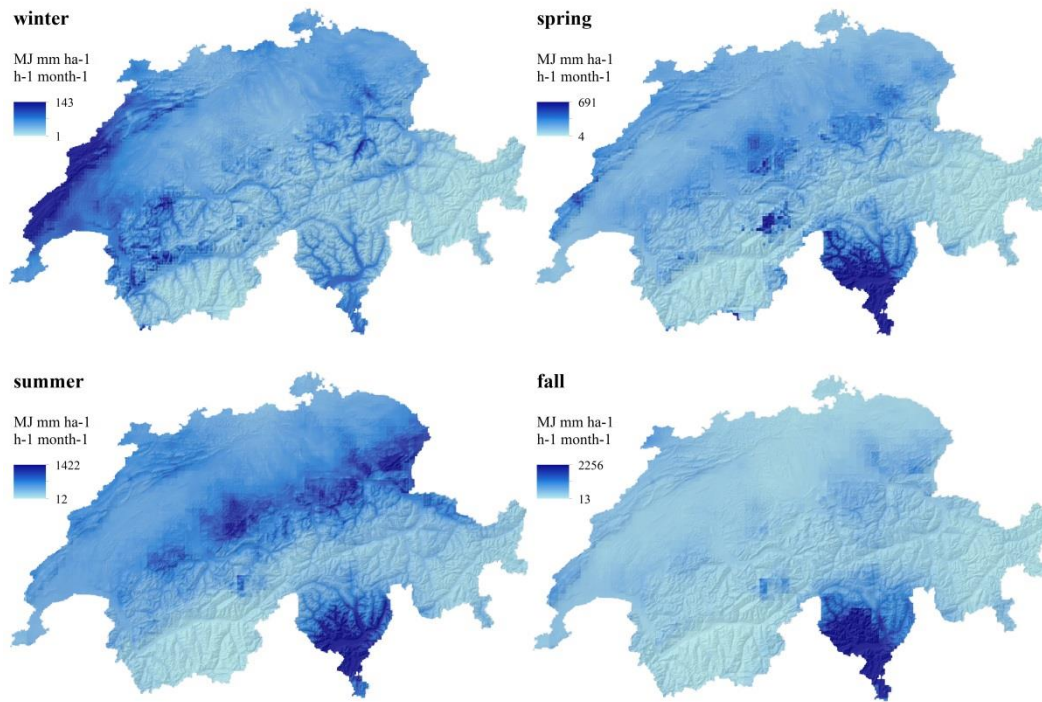
Figure 4: Seasonal rainfall erosivity maps for Switzerland derived by regression-kriging. The following months were averaged to derive seasonal maps: winter (Dec-Feb), spring (Mar-May), summer (Jun-Aug), fall (Sep-Nov).
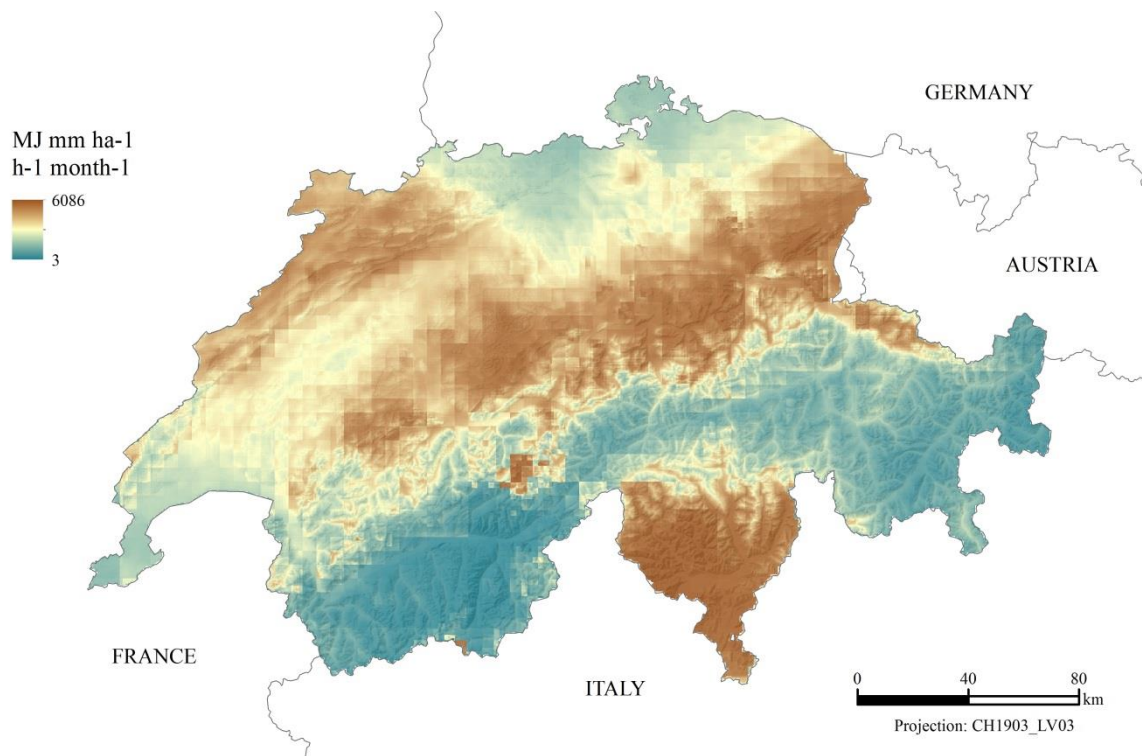
Figure 5: Range map (maximum R$_{mo}$ minus minimum R$_{mo}$) for Switzerland showing the variability of rainfall erosivity among a year.
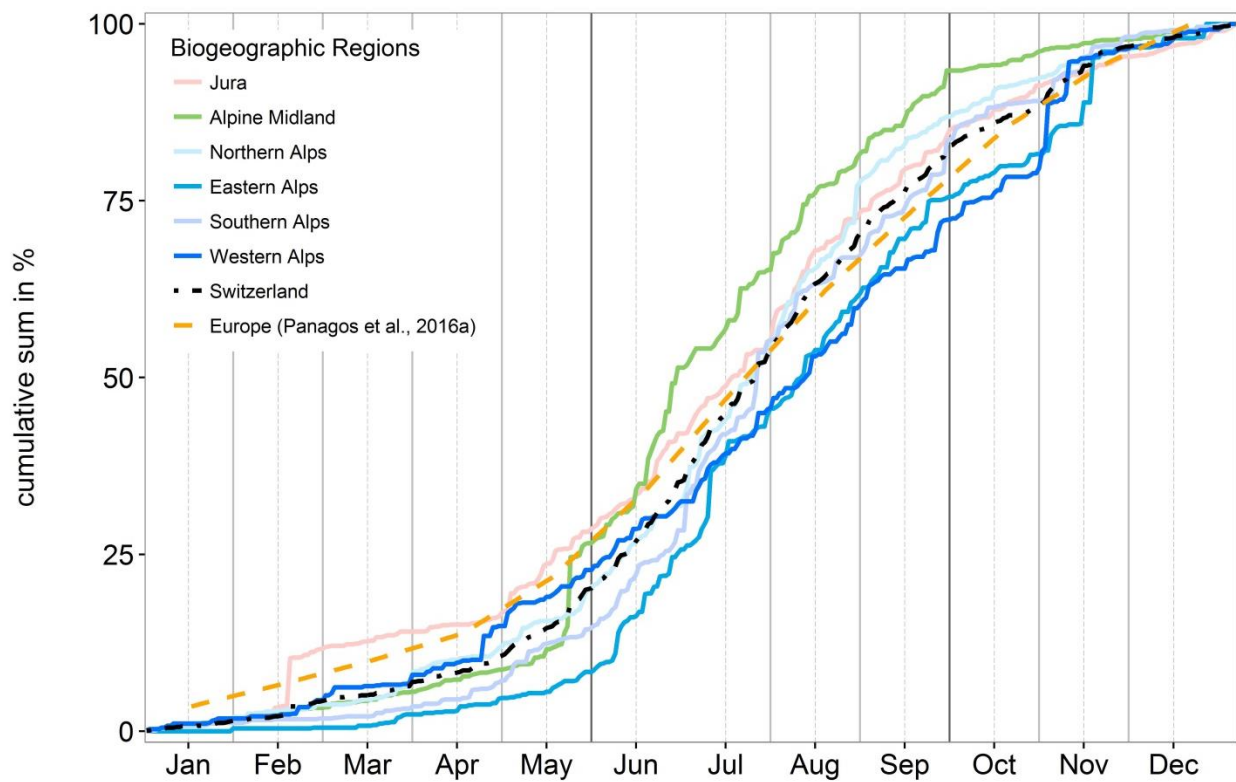
Figure 6: Cumulative daily rainfall erosivity proportion for Swiss biogeographic units, Switzerland and monthly rainfall erosivity for Europe (linear smoothed, European data from Panagos et al., 2016a).
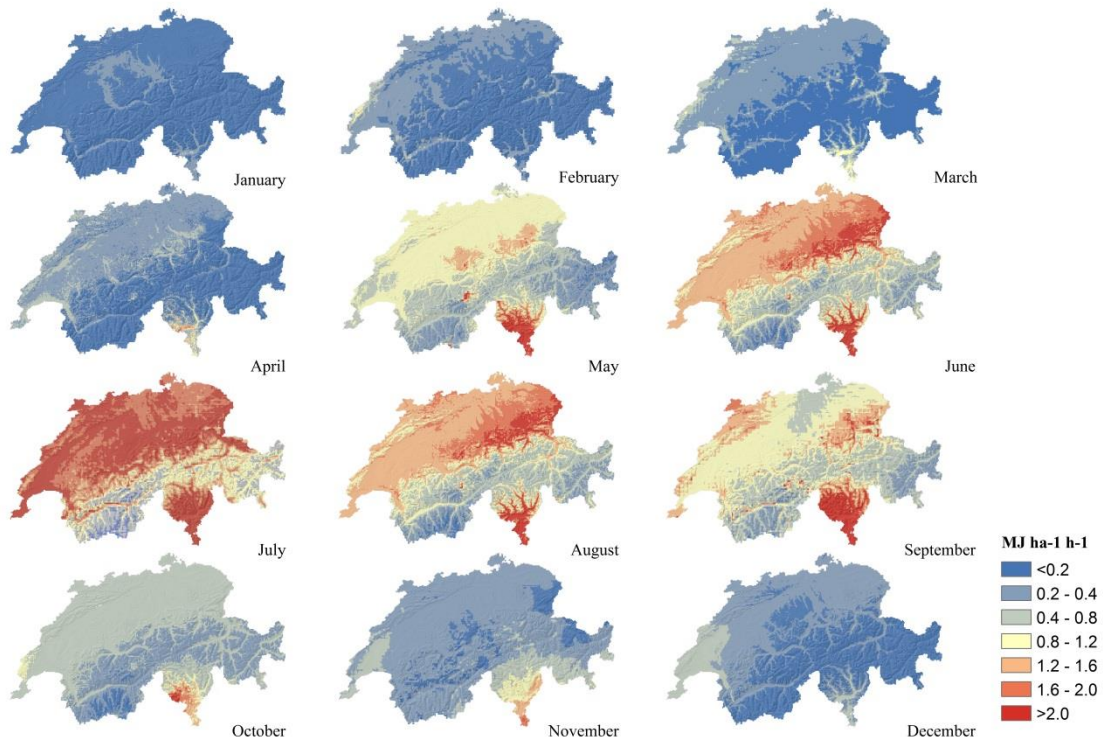
Figure 7: Monthly erosivity density (ED$_{mo}$) for Switzerland as ratio of monthly rainfall erosivity (R$_{mo}$) to monthly precipitation amount (P$_{mo}$ based on RhiresM).
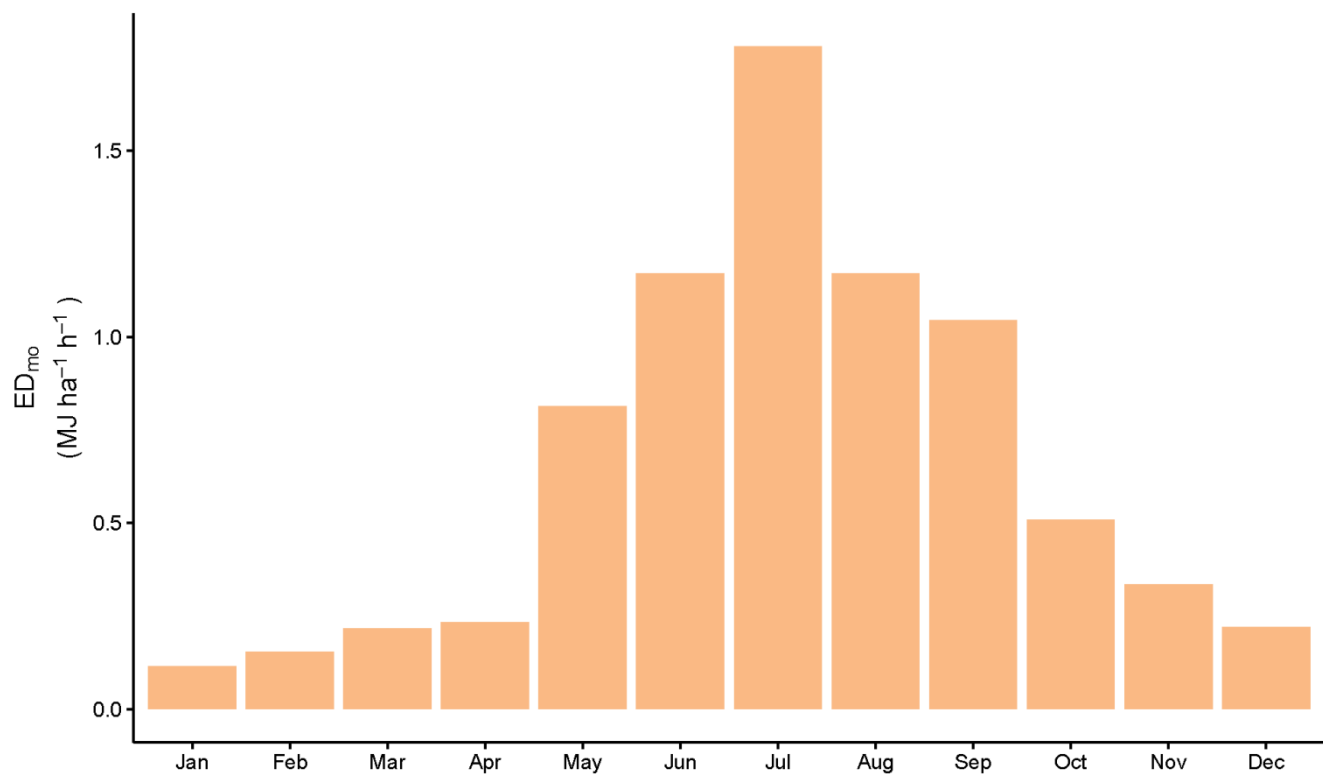
Figure 8: Mean monthly erosivity density (ED_{mo}) as ratios of R_{mo} (interpolated erosivity maps based on regression-kriging) to P_{mo} (precipitation sums from RhiresM) for Switzerland.